Circulation
Arrhythmia and Electrophysiology
JOURNAL OF THE AMERICAN HEART ASSOCIATION

Iron Overload Decreases $Ca_V1.3$-Dependent L-Type Ca^{2+} Currents Leading to Bradycardia, Altered Electrical Conduction, and Atrial Fibrillation

Robert A. Rose, Michael Sellan, Jeremy A. Simpson, Farzad Izaddoustdar, Carlo Cifelli, Brian K. Panama, Mark Davis, Dongling Zhao, Moniba Markhani, Geoffrey G. Murphy, Joerg Striessnig, Peter P. Liu, Scott P. Heximer and Peter H. Backx

Circ Arrhythm Electrophysiol 2011;4;733-742; originally published online July 11, 2011;
DOI: 10.1161/CIRCEP.110.960401
Circulation: Arrhythmia and Electrophysiology is published by the American Heart Association. 7272 Greenville Avenue, Dallas, TX 72514
 Print ISSN: 1941-3149. Online ISSN: 1941-3084

Iron Overload Decreases $Ca_V1.3$-Dependent L-Type Ca^{2+} Currents Leading to Bradycardia, Altered Electrical Conduction, and Atrial Fibrillation

Robert A. Rose, PhD*; Michael Sellan, MSc*; Jeremy A. Simpson, PhD*; Farzad Izaddoustdar, BSc; Carlo Cifelli, PhD; Brian K. Panama, PhD; Mark Davis, MD; Dongling Zhao, MSc; Moniba Markhani, BSc; Geoffrey G. Murphy, PhD; Joerg Striessnig, MD; Peter P. Liu, MD; Scott P. Heximer, PhD; Peter H. Backx, DVM, PhD

Background—Chronic iron overload (CIO) is associated with blood disorders such as thalassemias and hemochromatosis. A major prognostic indicator of survival in patients with CIO is iron-mediated cardiomyopathy characterized by contractile dysfunction and electrical disturbances, including slow heart rate (bradycardia) and heart block.

Methods and Results—We used a mouse model of CIO to investigate the effects of iron on sinoatrial node (SAN) function. As in humans, CIO reduced heart rate (≈20%) in conscious mice as well as in anesthetized mice with autonomic nervous system blockade and in isolated Langendorff-perfused mouse hearts, suggesting that bradycardia originates from altered intrinsic SAN pacemaker function. Indeed, spontaneous action potential frequencies in SAN myocytes with CIO were reduced in association with decreased L-type Ca^{2+} current ($I_{Ca,L}$) densities and positive (rightward) voltage shifts in $I_{Ca,L}$ activation. Pacemaker current (I_f) was not affected by CIO. Because $I_{Ca,L}$ in SAN myocytes (as well as in atrial and conducting system myocytes) activates at relatively negative potentials due to the presence of $Ca_V1.3$ channels (in addition to $Ca_V1.2$ channels), our data suggest that elevated iron preferentially suppresses $Ca_V1.3$ channel function. Consistent with this suggestion, CIO reduced $Ca_V1.3$ mRNA levels by ≈40% in atrial tissue (containing SAN) and did not lower heart rate in $Ca_V1.3$ knockout mice. CIO also induced PR-interval prolongation, heart block, and atrial fibrillation, conditions also seen in $Ca_V1.3$ knockout mice.

Conclusions—Our results demonstrate that CIO selectively reduces $Ca_V1.3$-mediated $I_{Ca,L}$, leading to bradycardia, slowing of electrical conduction, and atrial fibrillation as seen in patients with iron overload. **(*Circ Arrhythm Electrophysiol*. 2011;4:733-742.)**

Key Words: ion channels ■ action potentials ■ calcium channels ■ iron overload ■ cardiac electrophysiology ■ bradycardia ■ arrhythmias

The accumulation of excessive amounts of iron in tissues, including the heart, occurs under conditions of primary hemochromatosis (inherited) or hemosiderosis (secondary iron overload) and causes severe cardiac dysfunction, which is a leading cause of death in patients with iron overload.[1–4] Patients experiencing iron overload cardiomyopathies have impaired systolic and diastolic function often in conjunction with cardiac rhythm disturbances, including slowed electrical conduction, heart block, and increased susceptibility to atrial fibrillation.[5–8] Another common feature of patients with iron overload is a marked slowing of heart rate (ie, bradyarrhythmias).[1,9–11] Heart rate reductions along with altered electrical conduction also are prominent features of animal models of chronic iron overload.[12–15]

Clinical Perspective on p 742

Although the functional changes seen with iron overload are well documented, the molecular and physiological basis for the bradycardia and other electrical disturbances remain unknown. Because heart rate is a primary determinant of cardiac output and a key parameter used to regulate the cardiovascular system, bradycardia is predicted to contribute

Received October 18, 2009; accepted July 1, 2011.

From the Department of Physiology (R.A.R., M.S., J.A.S., F.I., C.C., B.K.P., M.D., D.Z., M.M., S.P.H., P.H.B.), Department of Medicine (R.A.R., M.S., J.A.S., F.I., B.K.P., M.D., M.M., P.P.L., P.H.B.), and Division of Cardiology (P.P.L., P.H.B.), University Health Network, University of Toronto, Toronto, Ontario, Canada; Molecular and Behavioral Neuroscience Institute, Department of Molecular and Integrative Physiology, University of Michigan Medical School, Ann Arbor, MI (G.G.M.); and Pharmacology and Toxicology, Institute of Pharmacy, University of Innsbruck, A-6020 Innsbruck, Austria (J.S.).

*Drs Rose, Sellan, and Simpson contributed equally to this work.

The online-only Data Supplement is available at http://circep.ahajournals.org/lookup/suppl/doi:10.1161/CIRCEP.110.960401/-/DC1.

Correspondence to Peter H. Backx, DVM, PhD, Room 68, Fitzgerald Bld, 150 College St, Toronto, Ontario M5S 3E2, Canada. E-mail: p.backx@utoronto.ca

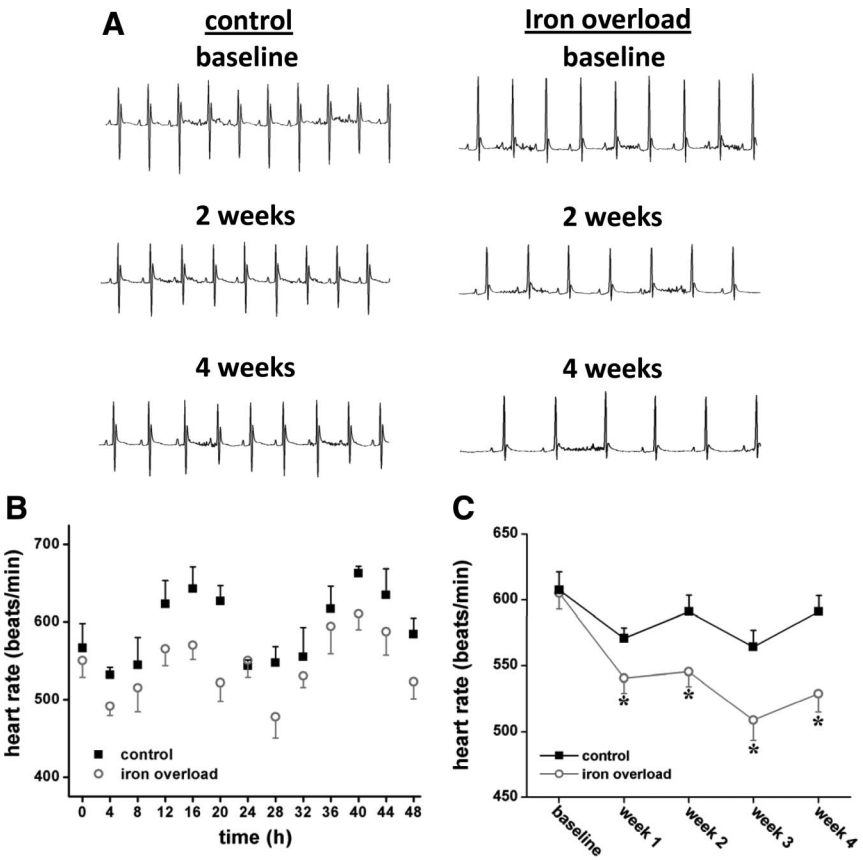

Figure 1. Effects of chronic iron overload on heart rate in conscious mice. **A**, Representative telemetry ECG recordings (1-s duration) before iron injection (ie, baseline) and after 2 and 4 weeks of injection with iron or placebo. Sample ECGs were measured at 2 PM (during mouse sleeping) to control for circadian rhythms. **B**, Heart rate measured every 4 hours over a consecutive 48-hour period, illustrating prominent circadian rhythms. **C**, Summary heart rate data averaged over a 4-week period in control conditions and after iron overload. For **B** and **C**, data are presented as mean±SEM (n=5 to 7 mice per group). *$P<0.05$ compared with control at the same time point analyzed by Student *t* test.

to cardiovascular changes, such as reduced blood pressure, typically observed in patients with iron overload.[16] Bradycardia in patients with iron overload could originate from factors extrinsic or intrinsic to the heart. For example, elevated iron could affect autonomic nervous system activity, possibly by impairing neuronal function[17] or interfering with other elements of the baroreceptor reflex pathways external to the heart.[18] Alternatively, intrinsic electrical activity of the specialized pacemaker myocytes located in the sinoatrial node (SAN)[19,20] could be disrupted by iron as a result of modulation of a number membrane currents,[21] Ca^{2+} handling,[22,23] or intracellular signaling.[24]

In the present study, we investigated the mechanisms by which chronic iron overload (CIO) slows heart rate using iron-overloaded mice. The data demonstrate that CIO causes pronounced heart rate slowing in association with other electrical changes, including PR-interval prolongation and heart block as well as impaired intrinsic firing rate of SAN myocytes and rightward shifts in L-type Ca^{2+} current ($I_{Ca,L}$) activation. These results suggest that bradycardia is caused by reductions in $Ca_V1.3$-based $I_{Ca,L}$ current, which is expressed (along with $Ca_V1.2$-based channels) in SAN, atria, and the cardiac conduction system but not working ventricles.[20] Indeed, CIO caused reductions in $Ca_V1.3$ mRNA but not $Ca_V1.2$ mRNA. Mice lacking $Ca_V1.3$ did not show reductions in heart rate or PR-interval prolongation when iron was elevated. Thus, we conclude that the slowing of heart rate and electrical conduction induced by iron overload is mediated by reductions in $Ca_V1.3$ expression. Some of these data have been presented in abstract form.[25]

Methods

An expanded Methods section is provided in the online-only Data Supplement.

Animals and Iron-Loading Protocol

Mice with CIO were generated as described previously[14] and in the online-only Data Supplement.

Electrocardiography

ECGs were recorded using telemetry in conscious mice or using body surface and intracardiac ECGs in anesthetized mice (see online-only Data Supplement).

Isolated SAN and Right Atrial Myocyte Electrophysiology

Single cardiomyocytes from the SAN or the right atrial appendage were isolated and used in patch-clamp studies as previously described[26–28] (see online-only Data Supplement for further details).

Statistics

All summary data are presented as mean±SEM. Results were considered statistically significant if $P<0.05$. *P* values were determined using paired or unpaired Student *t* tests, 1-way ANOVA, 1-way repeated-measures ANOVA, or rank sum tests (when the variance differed between groups). Actual *P* values are provided unless they were unavailable, as occurred when 1-way repeated-measures ANOVA or rank sum tests were applied to the data; thus, significance is indicated as $P<0.05$ or $P<0.001$ for nonparametric tests.

Results

After 4 weeks of iron loading,[14] iron levels in hearts of CIO mice were elevated ($P=6.1\times10^{-7}$) to 13.1±2.1 mg/g dry

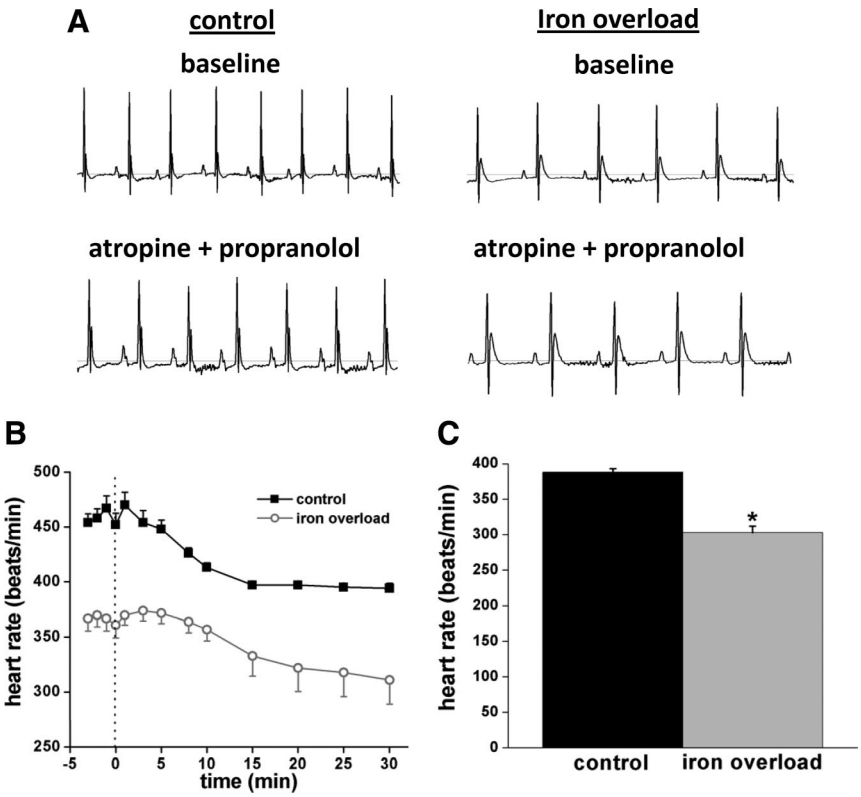

Figure 2. Effects of chronic iron overload on ECGs measured in anesthetized mice after autonomic nervous system blockade by intraperitoneal injection of atropine (1 mg/kg) and propranolol (10 mg/kg) and in isolated Langendorff-perfused hearts. **A**, Representative ECGs (1-s recordings) in control (left) and iron-overload mice at baseline (preinjection) as well as 25 minutes after injection of atropine and propranolol. **B**, Summary data showing heart rate at baseline and after autonomic nervous system blockade. Data are presented as mean±SEM (n=7 mice in each group). Heart rate was reduced ($P<0.05$) at all time points in iron-overload mice compared with controls (Student *t* test). **C**, Summary data showing averaged heart rates in isolated Langendorff-perfused hearts from control and iron-overload mice. Data are presented as mean±SEM (n=10 to 11 hearts per group). *$P<0.05$ versus control by Student *t* test.

weight compared to 0.55±0.1 mg/g dry weight measured in dextrose-injected (control) mice. CIO also caused reductions in systolic function (online-only Data Supplement Table 1 and Figure 1) and increases in the early/late (atrial) ventricular filling ratio (ie, E/A ratio). These results are identical to a previous report, which established that the iron accumulates in cardiomyocytes.[14] Although there were reductions in body weights ($P<0.001$) and heart weights ($P<0.001$) in CIO mice compared with control, there were no differences ($P=0.87$) in heart weight/body weight ratios (online-only Data Supplement Table 2). Similar to previous studies,[29] hepatic iron levels were elevated ($P<0.001$) to 73.1±6.8 mg/g dry weight in CIO mice compared with 0.41±0.1 mg/g dry weight for control mice in conjunction with increased liver weights ($P<0.001$) and liver weight/body weight ratios ($P<0.001$).

Figure 1 summarizes telemetry recordings in mice. Because heart rate fluctuates daily as a result of circadian influences, we measured ECGs every 4 hours over a 48-hour period each week. Figure 1**A** shows typical ECG recordings made during the sleeping period for mice before injection (ie, baseline) as well as 2 and 4 weeks after either placebo or iron injection. As expected, heart rate showed circadian fluctuations (Figure 1B). Iron injection for 2 weeks reduced heart rates without noticeably affecting diurnal sleep-wake fluctuations. Indeed, heart rates (averaged over 48 hours) progressively decreased as the period of iron injection was extended, with heart rates decreasing ($P<0.05$) from 605±12 beats/minute at baseline to 529±14 beats/minute after 4 weeks of CIO (Figure 1**C**). Placebo injection had no effect ($P=0.91$) on heart rate over the same 4-week period (607±14 versus 591±12 beats/minute at baseline). It is conceivable that these heart rate reductions contribute to the impaired cardiac contractility typically seen in this condition[1–5] because contractility increases with elevated heart rates (see Discussion).

The alterations in heart rate observed in CIO mice could arise from several mechanisms. For example, iron elevations could affect autonomic nerve activity[30] or directly influence properties of the SAN. To distinguish between these possibilities, ECGs were recorded in anesthetized mice with and without blockade of the autonomic nervous system, thereby allowing assessment of intrinsic SAN function.[26] As illustrated in Figure 2, intraperitoneal injection of atropine (1 mg/kg) plus propranolol (10 mg/kg) caused similar relative heart rate reductions in placebo (458±9 to 394±5 beats/minute) and iron-injected (367±12 to 311±22 beats/minute) mice. Consequently, heart rate remained reduced ($P<0.05$) in the anesthetized CIO mice compared with control mice after autonomic blockade. These results establish that bradycardia associated with iron overload results from impairment of the intrinsic properties of the SAN and further suggest that autonomic nerve function is not measurably altered by iron overload, consistent with the absence of alterations in circadian rhythms by elevated iron. Intrinsic changes in SAN firing were confirmed (Figure 2**C**) in isolated Langendorff-perfused hearts, which showed lower ($P=1\times10^{-7}$) heart rates when iron loaded (303±9 beats/minute) versus control (388±5 beats/minute). The similarity in heart rate between isolated hearts and mice injected with atropine and propranolols that complete autonomic blockade was achieved when mice were treated with these agents.

To explore the cellular basis for the iron-dependent changes in intrinsic SAN function, spontaneous action potentials (APs) were measured (Figure 3**A**) in isolated SAN myocytes (22°C to 23°C). The frequency of spontaneous APs

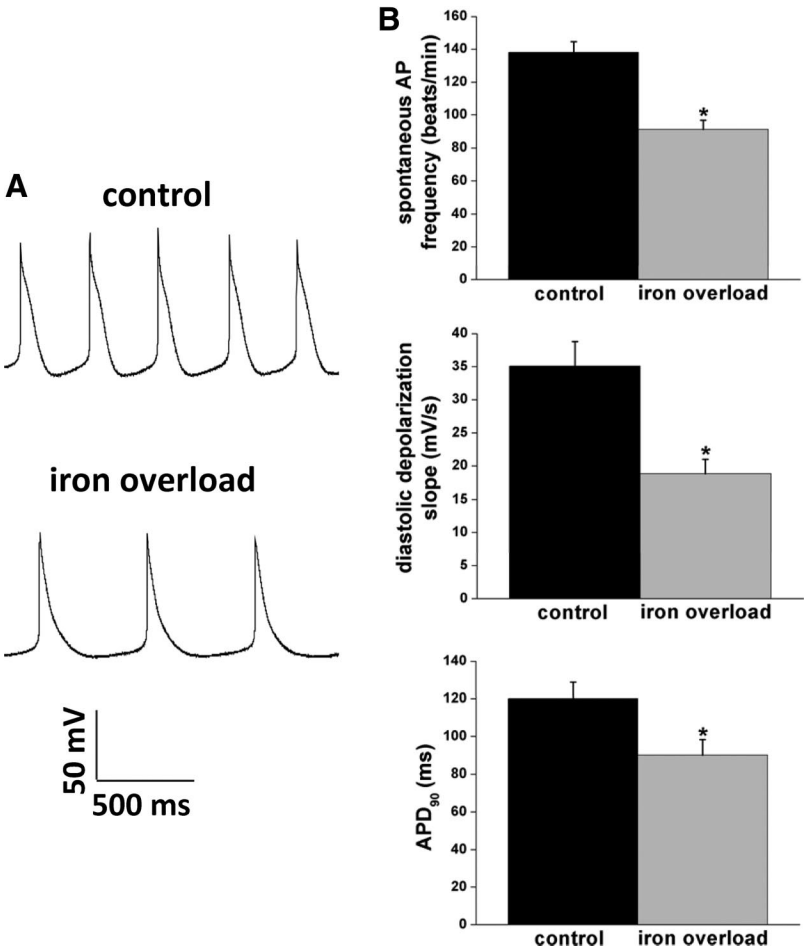

Figure 3. A, Representative spontaneous APs recorded from isolated sinoatrial node myocytes in control mice and mice subjected to iron overload. **B**, Summary data illustrating the effects of iron loading on spontaneous AP frequency, diastolic depolarization slope, and APD_{90}. Data are presented as mean±SEM (n=10 myocytes in each group). AP indicates action potential; APD_{90}, action potential duration at 90% repolarization. *$P<0.05$ versus control by Student *t* test. See also online-only Data Supplement Table 3.

(Figure 3**B**) was reduced ($P=3.0\times10^{-5}$) in SAN myocytes from CIO mice (91±5 beats/minute) compared with control (138±6 beats/minute). Detailed analysis of the AP profiles revealed that the slope of the diastolic depolarization (DD), a major determinant of firing frequency, was decreased ($P=3.1\times10^{-5}$) in SAN myocytes from CIO mice (Figure 3**B** and online-only Data Supplement Table 3). Elevated iron also reduced ($P=0.04$) the AP overshoot as well as AP durations at both 50% ($P=0.01$) and 90% ($P=0.02$) repolarization times. On the other hand, the maximum diastolic potential and AP upstroke velocity were not affected by iron (online-only Data Supplement Table 3).

Because the DD slope is a major determinant of spontaneous firing rate, we measured selected ionic currents expected to be active during the diastolic period (ie, hyperpolarization-activated pacemaker current [I_f] and $I_{Ca,L}$).[20] The density of I_f, measured at the end of 2-s voltage-clamp steps, did not differ ($P=0.87$) between control and CIO SAN myocytes, regardless of the voltage step used (Figure 4). This lack of effect of iron loading on I_f density between the groups is consistent with the absence of differences ($P=0.84$) in the maximum diastolic potentials (online-only Data Supplement Table 3) between CIO SAN myocytes (−68.1±1.6 mV) and control (−67.7±1.5 mV) during spontaneous AP firing. Next, we used voltage-clamp protocols designed to identify the 2 components of $I_{Ca,L}$ (ie, $Ca_V1.2$- and $Ca_V1.3$-based current) observed in myocytes of SAN, atria, and conducting systems.[31] Peak $I_{Ca,L}$ density (Figure 5) was reduced in CIO compared with control, particularly at negative membrane potentials. Specifically, $I_{Ca,L}$ densities in control SAN myocytes have the largest magnitude (−5.1±0.9 pA/pF) at ≈−10 mV. By contrast, the maximum $I_{Ca,L}$ magnitude (−2.6±0.2 pA/pF) was shifted to ≈+10 mV and was reduced ($P=0.006$) in CIO SAN myocytes compared with control. This voltage where $I_{Ca,L}$ peaks in CIO SAN myocytes is similar to voltages typically observed in ventricular myocytes (≈+10 mV), which only express $Ca_V1.2$-based $I_{Ca,L}$.[31] These observations suggest that iron preferentially reduces the more negatively activating $Ca_V1.3$-based $I_{Ca,L}$. To further quantify the changes in $I_{Ca,L}$ induced by iron, the steady-state conductance was calculated (Figure 5**C**). Maximum $I_{Ca,L}$ conductance in CIO SAN myocytes was reduced ($P=0.004$) to 71.7±2.3 pS/pF from 118.9±7.3 pS/pF in control SAN myocytes. Furthermore, the voltage required for 50% channel activation ($V_{1/2}$(act)) was shifted ($P=0.002$) from −21.9±3.1 mV in controls to −6.2±2.6 mV in CIO myocytes. Preferential reductions in $I_{Ca,L}$ at negative potentials induced by elevated iron readily explain the DD slope reductions observed during measurements of spontaneous AP firing.

Because $Ca_V1.3$ channels activate more negatively than $Ca_V1.2$ channels,[31] the positive shifts in $V_{1/2}$(act) of $I_{Ca,L}$ induced by iron suggest a preferential reduction in $Ca_V1.3$-mediated $I_{Ca,L}$. To test this suggestion, we measured $I_{Ca,L}$ in right atrial myocytes (Figure 5**D**), which also express $Ca_V1.3$.

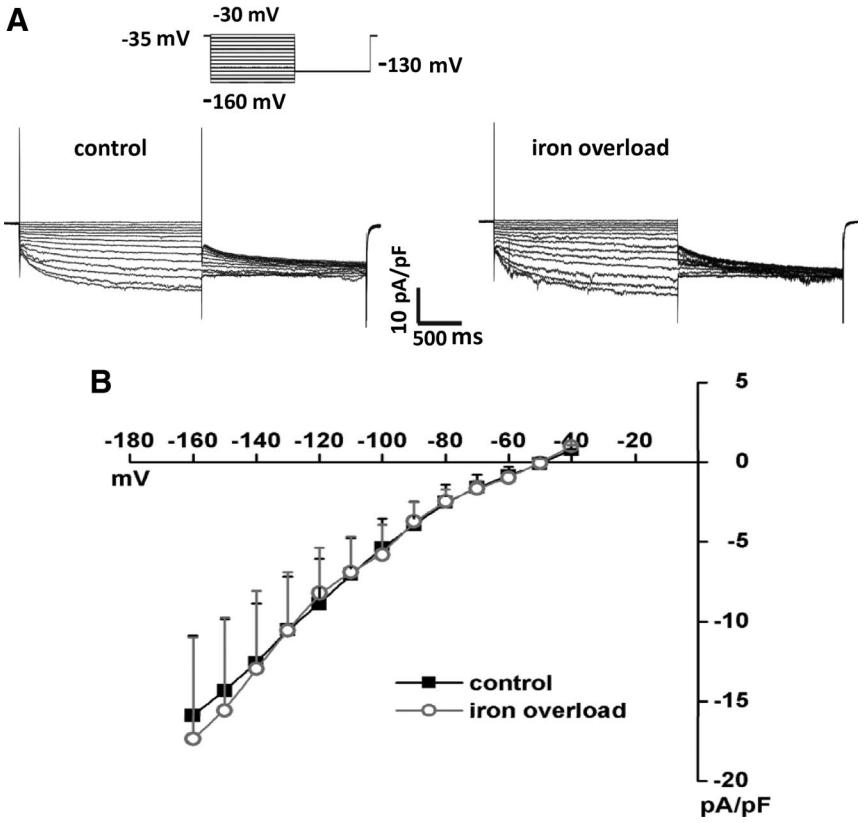

Figure 4. Properties of the hyperpolarization-activated current, I_f, in sinoatrial node myocytes from chronic iron-overload mice. **A**, Representative I_f recordings in sinoatrial node myocytes. Voltage-clamp protocol is shown in the inset. **B**, Summary I_f current-voltage curves showing no significant difference between control and iron-overload conditions. Data are presented as mean±SEM (n=5 control myocytes and n=6 iron-overload myocytes).

Similar to SAN myocytes but unlike ventricular myocytes,[14] peak $I_{Ca,L}$ was reduced (P=0.022) to −1.4±0.1 pA/pF in CIO right atrial myocytes from −2.5±0.3 pA/pF in control, whereas the voltage at which the maximal $I_{Ca,L}$ amplitude occurred was rightward shifted in CIO (Figure 5**E**). Indeed, maximum $I_{Ca,L}$ conductance (Figure 5**F**) was reduced (P=0.006) from 70.6±4.4 pS/pF in control atrial myocytes to 43.9±2.3 pS/pF in CIO myocytes, whereas the $V_{1/2}$(act) was right shifted (P=0.034) from −19.5±1.8 mV (control) to −13.6±1.6 mV (CIO).

Overall, these changes in CIO resemble closely those seen in $Ca_V1.3$-deficient mice,[32] supporting the conclusion that CIO preferentially reduces $Ca_V1.3$-mediated $I_{Ca,L}$ compared with $Ca_v1.2$ channels (see following). This conclusion is bolstered by our previous results that showed that CIO had only minor effects on $I_{Ca,L}$ density in ventricular myocytes,[14] which unlike SAN and atrial myocytes, do not express $Ca_V1.3$.[31–33] To interrogate this conclusion further, $Ca_V1.2$ and $Ca_V1.3$ expression levels (mRNA and protein) were measured in homogenates from the right atrium (including the SAN). Consistent with the iron-induced $I_{Ca,L}$ changes, $Ca_V1.3$ mRNA levels were >40% lower (P=0.018) in CIO compared with control (Figure 6). We tried to confirm these changes at the protein level, but these attempts failed (see online-only Data Supplement). By contrast, $Ca_V1.2$ mRNA trended toward reductions (P=0.336), whereas $Ca_V1.2$ protein was modestly reduced by ≈20% (Figure 6). Thus, we conclude that iron overload preferentially reduces $Ca_V1.3$-mediated currents, leading to reduced spontaneous firing rates of SAN myocytes.

If downregulation of $Ca_V1.3$-based $I_{Ca,L}$ is responsible for the observed effects of CIO, then heart rate reductions should not occur in mice lacking the $Ca_V1.3$ channel subunit. Consistent with previous reports,[32,34] heart rates in mice lacking $Ca_V1.3$ are lower (P<0.001) than in wild-type littermates (Figure 7). More importantly, iron overload caused heart rate increases (P<0.05) in $Ca_V1.3^{-/-}$ mice, which caused convergence of heart rates between the $Ca_V1.3^{-/-}$ and wild-type littermates during the iron injection period. Data beyond 3 weeks of iron injection are not shown because of relatively high mortality in both cohorts after 3 weeks of iron injection, which appears to be related to strain differences in response to iron. These findings support the conclusion that decreased $Ca_V1.3$-based channel expression is the dominant factor responsible for the heart rate reductions in iron overload.

In addition to being critical in setting spontaneous firing rates of SAN myocytes,[31,33] $Ca_V1.3$ α-subunits also regulate electrical conduction in hearts,[32,35] which was assessed in anesthetized mice using surface ECGs (with and without autonomic blockade), octapolar electrophysiology catheters, and isolated Langendorff-perfused hearts. As summarized in the Table, elevated iron altered several ECG parameters similar to iron overload patients[4] and gerbils.[12,13] For example, the durations of the P and QRS signals were prolonged in intracardiac recordings, possibly as a result of reductions in voltage-gated Na^+ currents (data not shown), as seen in gerbils.[21] More importantly, PR intervals were prolonged by iron overload in anesthetized mice and isolated hearts (Figure 8), indicating first-degree heart block. Intracardiac PR intervals also were prolonged (P=0.035) in CIO mice

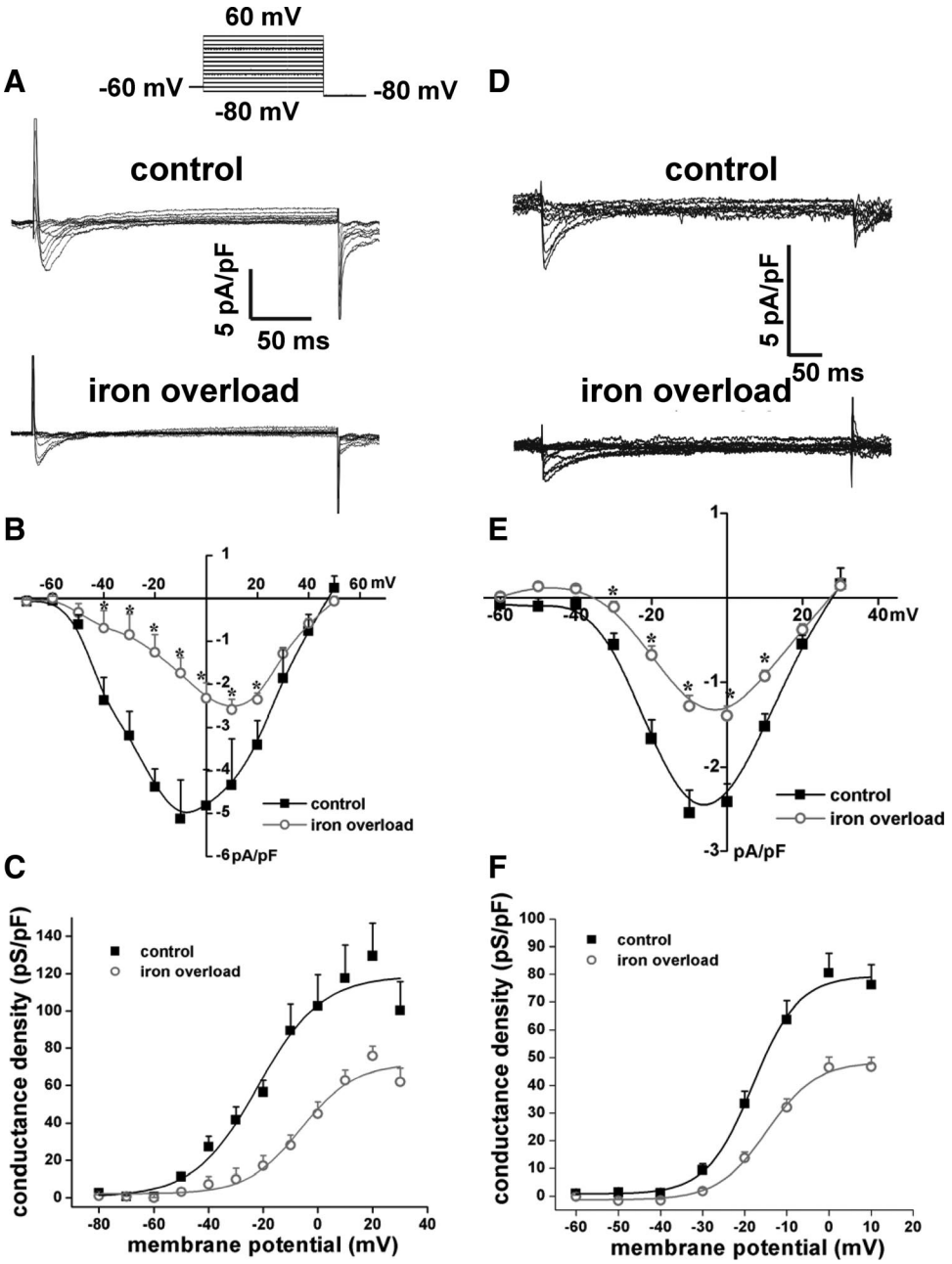

Figure 5. Effects of chronic iron overload on L-type Ca^{2+} current ($I_{Ca,L}$) in sinoatrial node (SAN) and right atrial myocytes. $Ca_V1.2$- and $Ca_V1.3$-dependent $I_{Ca,L}$ was measured simultaneously (see Methods and inset in **A**). **A**, Representative $I_{Ca,L}$ recordings in SAN myocytes. **B**, $I_{Ca,L}$ current-voltage curves in SAN myocytes. Data are presented as mean±SEM (n=8 myocytes for each group). *$P<0.05$ compared with control at the same membrane potential analyzed by Student *t* test. **C**, $I_{Ca,L}$ activation curves in SAN myocytes. **D**, Representative $I_{Ca,L}$ recordings in working right atrial myocytes. **E**, $I_{Ca,L}$ current-voltage curves in working right atrial myocytes. Data are presented as mean±SEM (n=7 atrial myocytes for control and n=11 atrial myocytes for iron overload). *$P<0.05$ compared with control at the same membrane potential analyzed by Student *t* test. **F**, $I_{Ca,L}$ activation curves in working right atrial myocytes.

(37.2±1.0 ms) compared with control (47.4±0.7 ms) in conjunction with longer AH intervals (Table), establishing slowing of conduction through the AV node and His bundle, as reported previously.[12] In addition, 2:1 AV-node block and sinus pauses (Figure 8) as well as prolonged ($P=0.006$) SAN recovery time (Table) were observed (Figure 8) in anesthetized CIO mice and with increased frequency after autonomic blockade (data not shown). None of these conduction disturbances were observed in control mice. Similar conduction and ECG changes have been documented in $Ca_V1.3$ knockout mice,[32,35] and elevated iron did not affect the PR interval in $Ca_V1.3$ knockout mice (Figure 7), supporting further the conclusion that the electrical disturbances induced by iron overload arise from reductions in $Ca_V1.3$-based $I_{Ca,L}$.

Discussion

The present mouse model of secondary iron overload reproduces the electrical changes observed in patients experiencing iron overload.[1,9–11] This model has been used by us[14] and others,[12,13,15] and leads to iron elevations in the liver and heart

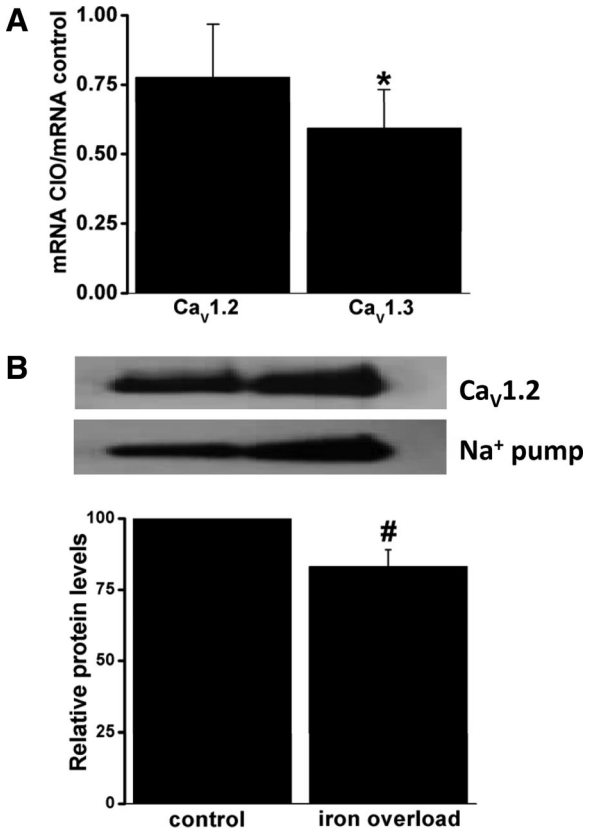

Figure 6. A, Real-time polymerase chain reaction measurements of mRNA level for the $Ca_V1.2$ and $Ca_V1.3$ α-subunits of the $I_{Ca,L}$ channels. The results show the ratio of mRNA in iron-loaded atria versus placebo control for $Ca_V1.2$ and $Ca_V1.3$ (n=5 for all groups). *$P<0.05$ compared with 1 using the Student *t* test. **B**, Representative western blot for $Ca_V1.2$ and Na^+/K^+ ATPase (loading control) in atria isolated (top) along with the relative protein expression levels of $Ca_V1.2$ normalized by the level of Na^+ pump expression for control and iron-overload atria (n=3 for control and iron overload). #$P<0.05$ relative to control, Student *t* test.

similar to humans with advanced iron overload. Our investigations revealed a pronounced bradycardia in CIO mice, as is seen in patients with iron overload.[1,9–11] Bradycardia could contribute to the impaired cardiac contractility seen with CIO[4,5,8,14] (independent of the effects of iron on myocardial contractility and cardiac fibrosis[4,5,8,14]) as a consequence of the force-frequency relationship, which varies between mouse strains.[36] Regardless, the present results show that the bradycardia in CIO results from slowing of the spontaneous activity of the SAN in association with changes in AP properties. These electrical changes were tightly linked (see following) to $I_{Ca,L}$ reductions and rightward shifts in $I_{Ca,L}$ activation consistent with preferential reduction in $Ca_V1.3$- versus $Ca_V1.2$-dependent $I_{Ca,L}$. CIO did not cause changes in I_f current. These observations support the conclusion that the reductions in heart rate as well as the PR-interval prolongation, heart block, and conduction deficits seen in iron overload result from selective reductions in $Ca_V1.3$-mediated $I_{Ca,L}$. Indeed, CIO did not cause heart rate reductions or PR-interval prolongation in mice lacking $Ca_V1.3$. In addition, lower heart rates observed in $Ca_V1.3^{-/-}$ mice compared with wild-type littermates[31,37] were abolished by iron treatment, supporting the conclusion that $Ca_V1.3$ reductions are, indeed, the primary cause of heart rate reductions in iron overload.

The reductions of $I_{Ca,L}$ in SAN and atrial myocytes induced by CIO were initially somewhat surprising because $I_{Ca,L}$ density is not measurably altered in ventricular myocytes from CIO mice.[14] However, $I_{Ca,L}$ in SAN and atria myocytes arises from both $Ca_V1.2$ and $Ca_V1.3$ L-type channels, whereas ventricular myocytes only express $Ca_V1.2$ subunits,[31–33] suggesting that the $I_{Ca,L}$ reductions observed in iron-loaded SAN and atrial myocytes may result from differential reduction in $Ca_V1.3$-mediated $I_{Ca,L}$. Consistent with this suggestion, the mRNA levels of $Ca_V1.3$ were reduced by ≈40% in right atria. Because whole atria included the SAN, we infer that reductions in $Ca_V1.3$ occur in both atrial and SAN myocytes after iron loading. On the other hand, $Ca_V1.2$ mRNA levels were unaffected by iron, although protein was slightly reduced. The connection between preferential reductions in $Ca_V1.3$-based $I_{Ca,L}$ is further supported by the large rightward shifts in $V_{1/2}$(act) for $I_{Ca,L}$ activation and in the voltage of the maximal $I_{Ca,L}$ amplitude in myocytes from SAN and atria because $Ca_V1.3$ channels activate at more negative potentials (≈−50 mV) than $Ca_V1.2$-mediated $I_{Ca,L}$ (≈−30 mV).[31] Moreover, SAN and AV node myocytes express relatively more $Ca_V1.3$ channels than atrial cells, which given the differential effects of iron on $Ca_V1.3$ channels, explains the larger effects of iron overload on $I_{Ca,L}$ in the present SAN myocytes versus atrial myocytes. Selective loss of $Ca_V1.3$-mediated $I_{Ca,L}$ is further supported by the observation that the voltage dependence of $I_{Ca,L}$ in atrial and SAN myocytes after iron are similar to that typically seen in ventricular myocytes.[38]

Selective reductions in $Ca_V1.3$-dependent $I_{Ca,L}$ readily explains reduced spontaneous firing rates of SAN myocytes and, thereby, heart rate slowing of in vivo and isolated hearts with iron overload. Indeed, we found that mice lacking $Ca_V1.3$ channels have reduced heart rates and slow spontaneous firing rates in isolated SAN-atrial preparations compared with wild-type littermates, as reported previously.[31,33] Moreover, heart rates actually increased in iron-overload $Ca_V1.3$ knockout mice, possibly as a result of impairment of heart function and the cardiomyopathy induced by CIO,[4,14] which is expected to induce compensatory changes in autonomic nerve activity. Presumably excessive iron causes reductions in DD slope because of reduced $Ca_V1.3$-dependent $I_{Ca,L}$ currents, particularly at voltages between −50 and −20 mV where the $Ca_V1.3$ channel activates. These reduced slopes delay the time required for membrane potentials to reach the threshold for $Ca_V1.2$-dependent $I_{Ca,L}$, thereby depressing spontaneous firing rates. Consistent with this conclusion, $Ca_V1.3$ knockout mice also showed lower DD slopes in association with reduced heart rates.[31]

Based on previous findings in SAN myocytes,[39] the $I_{Ca,L}$ changes also can explain reduced AP amplitudes and durations in SAN myocytes. Although it is conceivable that changes in other currents also occur in iron overload, such as the changes in Na^+ current and transient outward potassium current seen in ventricular myocytes of gerbils,[21] the relevance of these changes is unclear because SAN myocytes

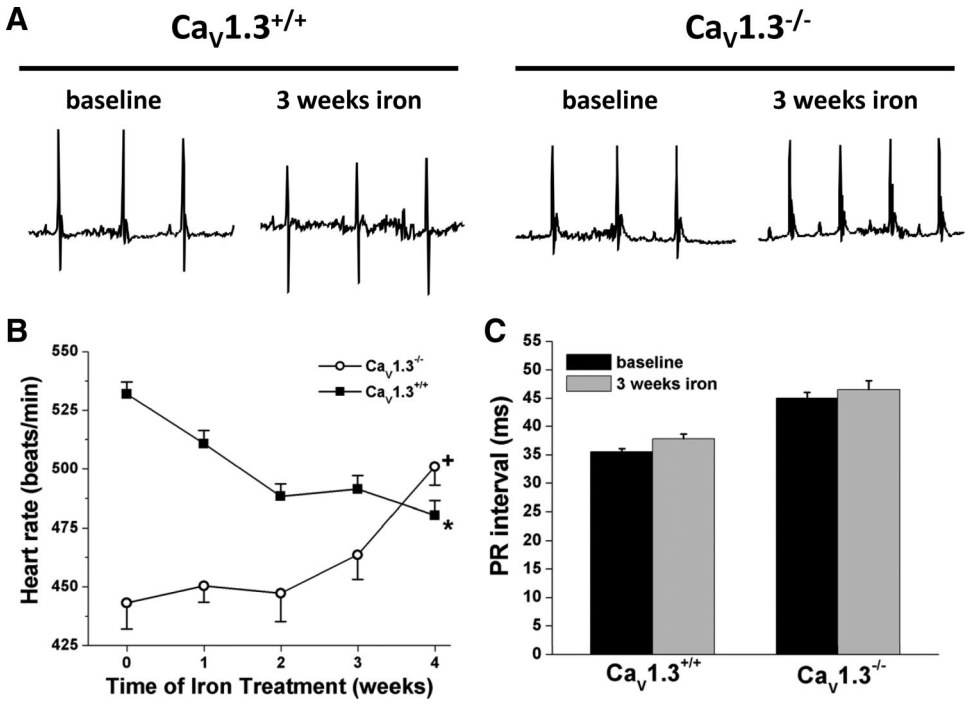

Figure 7. Effects of iron treatment in conscious $Ca_V1.3$ knockout mice. **A**, Representative telemetry ECGs (0.5-s recordings) before (baseline) and after (3 weeks) iron injection in $Ca_V1.3$ knockout and littermate wild-type mice. All sample ECGs were measured at 2 PM (sleep time). **B**, heart rates averaged over a 48-hour period (measured every 4 hours) for $Ca_V1.3$ knockout and littermate wild-type mice showing increases in heart rate for $Ca_V1.3$ knockout mice but decreases in wild-type littermate controls. **C**, Summary of PR intervals after 3 weeks of iron injection in $Ca_V1.3$ knockout and littermate wild-type mice. For **B** and **C**, data are presented as mean±SEM (n>7 mice per group). +$P<0.001$ compared to baseline (time=0) analyzed by Kruskal-Wallis test with Dunn post hoc analysis. *$P<0.05$ compared to wild-type littermates at the same time point using Student *t* test.

have relatively low densities of Na^+ and transient outward potassium currents.[39,40]

In addition to bradycardia, iron overload causes other electrical disturbances.[5,7,8,41] In the present CIO mice, we reproducibly observed sinus pauses, prolonged PR intervals, and second-degree heart block. Interestingly, these conduction disturbances also are seen in $Ca_V1.3$ knockout mice.[32,33,35,42] PR-interval prolongation and second-degree heart block are because $Ca_V1.3$ channels are expressed in the AV node[31,43] where they are critical for electrical conduction.[35,42] In fact, disturbances of AV conduction and heart block are seen both in $Ca_V1.3$ knockout mice[32,35] and in congenital heart block, a condition linked to elevated maternal antibodies to $Ca_V1.3$ channels that block $Ca_V1.3$-dependent $I_{Ca,L}$.[43]

Table. Intracardiac ECG Parameters From Control and Iron-Overload Mice

	Control (n=7)	Iron Overload (n=5)	*P*
R-R interval	124±5	158±7*	0.0032
PR interval	39.8±1.0	43.6±1.2†	0.0346
P-wave width	16.4±0.5	20.3±0.8*	0.0012
AH	25.7±0.7	29.2±1.4†	0.0397
HV interval	12.3±0.5	12.00±0.5	0.633
QRS	10.8±0.5	11.3±0.5	0.493
QT_C	41.9±0.9	48.2±1.4*	0.0027
cSNRT	26.4±4.7	62.0±10.3*	0.0059
AVNERP	60.3±2.6	63.4±7.7	0.6694
AV_W	78.4±2.3	88.8±5.5	0.0815
VERP	17.9±2.8	44.4±4.9‡	0.0005

Data are presented as mean±SEM measured in ms. Data were analyzed with Student *t* test. AH indicates the interval from the start of the P wave to the start of the His bundle signal (ie, H signal); AVNERP, AV node effective refractory period; AV_W, induction of Wenckebach AV node block; cSNRT, corrected sinus node recovery time; QTc, corrected QT interval; VERP, ventricular effective refractory period.

*$P<0.01$ vs control.

†$P<0.05$ vs control.

‡$P<0.001$ vs control.

Previous studies have established that decreased $I_{Ca,L}$ density occurs in atrial myocytes from humans[44] and animals models[45] with atrial fibrillation, with reductions in both $Ca_V1.2$ and $Ca_V1.3$ expression being linked to atrial fibrillation in humans.[46] A reduction in $Ca_V1.3$ channels seems particularly relevant because $Ca_V1.3$ knockout mice are susceptible to atrial fibrillation.[42] Atrial fibrillation also has been associated with CIO.[34] Our results, therefore, suggest that atrial fibrillation in patients with iron overload could arise from a reduction in $Ca_V1.3$-based $I_{Ca,L}$. Indeed, although atrial fibrillation was not seen in conscious telemetric-implanted CIO mice, stable rotors could be induced in 2 of 10 isolated atrial preparations obtained from iron-overload mice, whereas the sensitivity of isolated atria to atrial fibrillation induction in the presence of the parasympathomimetic carbachol was shifted to lower concentrations by iron overload (online-only Data Supplement Figure 2). Clearly, additional studies will be required

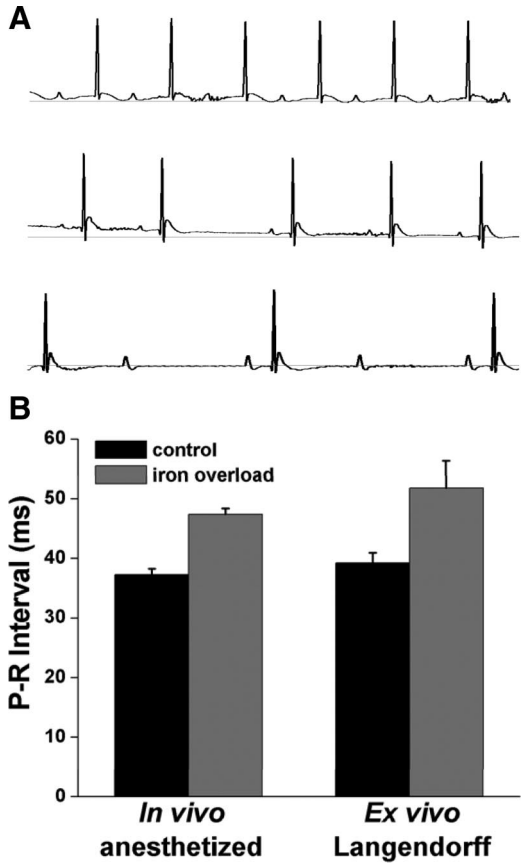

Figure 8. A, Representative ECG recordings illustrating conduction disturbances observed in anesthetized chronic iron-overload mice after 3 weeks of iron injection: top trace shows PR-interval prolongation (first-degree AV node block), middle trace shows typical sinus pauses, and bottom trace 2:1 AV node block. No conduction disturbances were observed in control mice. **B**, Average PR intervals at baseline (before iron injection) and after 3 weeks of iron injection in anesthetized mice and hearts excised from iron-overload mice.

to more fully assess possible connections between iron-induced changes of $Ca_V1.3$-mediated $I_{Ca,L}$ and atrial fibrillation in patients with iron overload.

The precise mechanisms by which iron overload inhibits $I_{Ca,L}$ in the SAN and atria are not clear. The *$Ca_V1.3$* gene does not have an iron-response element in its promoter.[4] On the other hand, iron overload induces oxidative damage and increases fibrosis,[4] which could contribute to alterations in heart rates and electrical conduction. Elevated iron also could conceivably alter channel properties like permeation and gating properties, as we reported previously.[38] The fact that some currents are reduced ($I_{Ca,L}$ in SAN and atrial myocytes, Na^+ current in ventricular myocytes[21]), whereas others are unaffected ($I_{Ca,L}$ in ventricular myocytes[14]) or even increased (transient outward potassium current in ventricular myocytes[21]), suggests that nonspecific oxidative damage to ion channel proteins is not the only factor involved in the iron-induced remodeling that occurs with iron overload.

In conclusion, the present results establish that iron overload in mice leads to decreased $Ca_V1.3$-based $I_{Ca,L}$ in SAN and atrial myocytes. These changes explain the development of sinus bradycardia, slowed electrical conduction, and increased susceptibility to atrial fibrillation in mice as well as in human iron overload. Future studies will be needed to assess whether preventing reductions in $Ca_V1.3$ channel proteins alleviates the electrical remodeling and increased susceptibility to arrhythmias seen in patients with iron overload.

Acknowledgments

We thank Wallace Yang for technical assistance.

Sources of Funding

This study was supported by the Canadian Institutes for Health Research (CIHR) (MOP 79460 to Dr Backx). Dr Backx is a Career Investigator of the Heart and Stroke Foundation of Ontario. Dr Murphy acknowledges funding from National Institute on Aging R01 AG028488. Dr Heximer holds a Canada Research Chair. Dr Striessnig acknowleges funding from the Austrian Science Fund (P20670). Dr Cifelli is the recipient of a CIHR Graduate Scholarship. Dr Rose is a CIHR New Investigator supported by operating grants from the CIHR (MOP 93718) and the Heart and Stroke Foundation of Nova Scotia.

Disclosures

None.

References

1. Buja LM, Roberts WC. Iron in the heart. Etiology and clinical significance. *Am J Med*. 1971;51:209–221.
2. Engle MA, Erlandson M, Smith CH. Late cardiac complications of chronic, severe, refractory anemia with hemochromatosis. *Circulation*. 1964;30:698–705.
3. Liu P, Olivieri N. Iron overload cardiomyopathies: new insights into an old disease. *Cardiovasc Drugs Ther*. 1994;8:101–110.
4. Oudit GY, Trivieri MG, Khaper N, Liu PP, Backx PH. Role of L-type Ca^{2+} channels in iron transport and iron-overload cardiomyopathy. *J Mol Med*. 2006;84:349–364.
5. Aessopos A, Farmakis D, Karagiorga M, Voskaridou E, Loutradi A, Hatziliami A, Joussef J, Rombos J, Loukopoulos D. Cardiac involvement in thalassemia intermedia: a multicenter study. *Blood*. 2001;97:3411–3416.
6. Davis MJ, Wu X, Nurkiewicz TR, Kawasaki J, Gui P, Hill MA, Wilson E. Regulation of ion channels by protein tyrosine phosphorylation. *Am J Physiol*. 2001;281:H1835–H1862.
7. Lombardo T, Tamburino C, Bartoloni G, Morrone ML, Frontini V, Italia F, Cordaro S, Privitera A, Calvi V. Cardiac iron overload in thalassemic patients: an endomyocardial biopsy study. *Ann Hematol*. 1995;71:135–141.
8. Schellhammer PF, Engle MA, Hagstrom JW. Histochemical studies of the myocardium and conduction system in acquired iron-storage disease. *Circulation*. 1967;35:631–637.
9. Horwitz LD, Rosenthal EA. Iron-mediated cardiovascular injury. *Vasc Med*. 1999;4:93–99.
10. Rosenqvist M, Hultcrantz R. Prevalence of a haemochromatosis among men with clinically significant bradyarrhythmias. *Eur Heart J*. 1989;10:473–478.
11. Wang TL, Chen WJ, Liau CS, Lee YT. Sick sinus syndrome as the early manifestation of cardiac hemochromatosis. *J Electrocardiol*. 1994;27:91–96.
12. Laurita KR, Chuck ET, Yang T, Dong WQ, Kuryshev YA, Brittenham GM, Rosenbaum DS, Brown AM. Optical mapping reveals conduction slowing and impulse block in iron-overload cardiomyopathy. *J Lab Clin Med*. 2003;142:83–89.
13. Obejero-Paz CA, Yang T, Dong WQ, Levy MN, Brittenham GM, Kuryshev YA, Brown AM. Deferoxamine promotes survival and prevents electrocardiographic abnormalities in the gerbil model of iron-overload cardiomyopathy. *J Lab Clin Med*. 2003;141:121–130.
14. Oudit GY, Sun H, Trivieri MG, Koch SE, Dawood F, Ackerley C, Yazdanpanah M, Wilson GJ, Schwartz A, Liu PP, Backx PH. L-type Ca^{2+} channels provide a major pathway for iron entry into cardiomyocytes in iron-overload cardiomyopathy. *Nat Med*. 2003;9:1187–1194.

15. Schwartz KA, Li Z, Schwartz DE, Cooper TG, Braselton WE. Earliest cardiac toxicity induced by iron overload selectively inhibits electrical conduction. *J Appl Physiol*. 2002;93:746–751.
16. Veglio F, Melchio R, Rabbia F, Molino P, Genova GC, Martini G, Schiavone D, Piga A, Chiandussi L. Blood pressure and heart rate in young thalassemia major patients. *Am J Hypertens*. 1998;11:539–547.
17. Madsen E, Gitlin JD. Copper and iron disorders of the brain. *Ann Rev Neurosci*. 2007;30:317–337.
18. Cardoso LM, Pedrosa ML, Silva ME, Moraes MF, Colombari E, Chianca DA Jr. Baroreflex function in conscious rats submitted to iron overload. *Braz J Med Biol Res*. 2005;38:205–214.
19. Irisawa H, Brown HF, Giles W. Cardiac pacemaking in the sinoatrial node. *Physiol Rev*. 1993;73:197–227.
20. Mangoni ME, Nargeot J. Genesis and regulation of the heart automaticity. *Physiol Rev*. 2008;88:919–982.
21. Kuryshev YA, Brittenham GM, Fujioka H, Kannan P, Shieh CC, Cohen SA, Brown AM. Decreased sodium and increased transient outward potassium currents in iron-loaded cardiac myocytes. Implications for the arrhythmogenesis of human siderotic heart disease. *Circulation*. 1999; 100:675–683.
22. Kim E, Giri SN, Pessah IN. Iron(II) is a modulator of ryanodine-sensitive calcium channels of cardiac muscle sarcoplasmic reticulum. *Toxicol Appl Pharmacol*. 1995;130:57–66.
23. Stoyanovsky DA, Salama G, Kagan VE. Ascorbate/iron activates Ca^{2+}-release channels of skeletal sarcoplasmic reticulum vesicles reconstituted in lipid bilayers. *Arch Biochem Biophys*. 1994;308:214–221.
24. Lesnefsky EJ, Ye J. Exogenous intracellular, but not extracellular, iron augments myocardial reperfusion injury. *Am J Physiol*. 1994;266: H384–H392.
25. Sellan M, Rose RA, Ciffeli C, Heximer SP, Backx PH. Chronic iron-overload causes sinus bradycardia by altering electrical activity in sino-atrial node myocytes. *Biophys J*. 2009;96:259a–260a.
26. Rose RA, Kabir MG, Backx PH. Altered heart rate and sinoatrial node function in mice lacking the cAMP regulator phosphoinositide 3-kinase-gamma. *Circ Res*. 2007;101:1274–1282.
27. Rose RA, Lomax AE, Kondo CS, Anand-Srivastava MB, Giles WR. Effects of C-type natriuretic peptide on ionic currents in mouse sinoatrial node: a role for the NPR-C receptor. *Am J Physiol*. 2004;286: H1970–H1977.
28. Cifelli C, Rose RA, Zhang H, Voigtlaender-Bolz J, Bolz SS, Backx PH, Heximer SP. RGS4 Regulates Parasympathetic signaling and heart rate control in the sinoatrial node. *Circ Res*. 2008;103:527–535.
29. Yang T, Brittenham GM, Dong WQ, Levy MN, Obejero-Paz CA, Kuryshev YA, Brown AM. Deferoxamine prevents cardiac hypertrophy and failure in the gerbil model of iron-induced cardiomyopathy. *J Lab Clin Med*. 2003;142:332–340.
30. Kardelen F, Tezcan G, Akcurin G, Ertug H, Yesilipek A. Heart rate variability in patients with thalassemia major. *Pediatr Cardiol*. 2008;29: 935–939.
31. Mangoni ME, Couette B, Bourinet E, Platzer J, Reimer D, Striessnig J, Nargeot J. Functional role of L-type Cav1.3 Ca2+ channels in cardiac pacemaker activity. *Proc Natl Acad Sci U S A*. 2003;100:5543–5548.
32. Zhang Z, He Y, Tuteja D, Xu D, Timofeyev V, Zhang Q, Glatter KA, Xu Y, Shin HS, Low R, Chiamvimonvat N. Functional roles of Cav1.3(alpha1D) calcium channels in atria: insights gained from gene-targeted null mutant mice. *Circulation*. 2005;112:1936–1944.
33. Zhang Z, Xu Y, Song H, Rodriguez J, Tuteja D, Namkung Y, Shin HS, Chiamvimonvat N. Functional roles of Ca(v) 1.3 (alpha(1D)) calcium channel in sinoatrial nodes: insight gained using gene-targeted null mutant mice. *Circ Res.* 2002;90:981–987.
34. Zacharski LR, McKernan L, Metzger ME, Malone MG, Samnotra V, Bhargava A, Steiner PR, Rauwerdink CA, Ornstein DL, Cornell CJ. Remission of paroxysmal atrial fibrillation with iron reduction in haemophilia A. *Haemophilia*. 2010;16:726–730.
35. Matthes J, Yildirim L, Wietzorrek G, Reimer D, Striessnig J, Herzig S. Disturbed atrio-ventricular conduction and normal contractile function in isolated hearts from Cav1.3-knockout mice. *Naunyn Schmiedebergs Arch Pharmacol*. 2004;369:554–562.
36. Stull LB, Hiranandani N, Kelley MA, Leppo MK, Marban E, Janssen PM. Murine strain differences in contractile function are temperature- and frequency-dependent. *Pflugers Arch*. 2006;452:140–145.
37. Platzer J, Engel J, Schrott-Fischer A, Stephan K, Bova S, Chen H, Zheng H, Striessnig J. Congenital deafness and sinoatrial node dysfunction in mice lacking class D L-type Ca^{2+} channels. *Cell*. 2000;102:89–97.
38. Tsushima RG, Wickenden AD, Bouchard RA, Oudit GY, Liu PP, Backx PH. Modulation of iron uptake in heart by L-type Ca^{2+} channel modifiers: possible implications in iron overload. *Circ Res*. 1999;84: 1302–1309.
39. Dobrzynski H, Boyett MR, Anderson RH. New insights into pacemaker activity: promoting understanding of sick sinus syndrome. *Circulation*. 2007;115:1921–1932.
40. Lei M, Zhang H, Grace AA, Huang CL. SCN5A and sinoatrial node pacemaker function. *Cardiovasc Res*. 2007;74:356–365.
41. Davis BA, Porter JB. Long-term outcome of continuous 24-hour deferoxamine infusion via indwelling intravenous catheters in high-risk beta-thalassemia. *Blood*. 2000;95:1229–1236.
42. Mancarella S, Yue Y, Karnabi E, Qu Y, El-Sherif N, Boutjdir M. Impaired Ca^{2+} homeostasis is associated with atrial fibrillation in the alpha1D L-type Ca^{2+} channel KO mouse. *Am J Physiol*. 2008;295: H2017–H2024.
43. Qu Y, Baroudi G, Yue Y, Boutjdir M. Novel molecular mechanism involving alpha1D (Cav1.3) L-type calcium channel in autoimmune-associated sinus bradycardia. *Circulation*. 2005;111:3034–3041.
44. Van Wagoner DR, Pond AL, Lamorgese M, Rossie SS, McCarthy PM, Nerbonne JM. Atrial L-type Ca^{2+} currents and human atrial fibrillation. *Circ Res*. 1999;85:428–436.
45. Yue L, Feng J, Gaspo R, Li GR, Wang Z, Nattel S. Ionic remodeling underlying action potential changes in a canine model of atrial fibrillation. *Circ Res*. 1997;81:512–525.
46. Gaborit N, Steenman M, Lamirault G, Le MN, Le BS, Lande G, Leger J, Charpentier F, Christ T, Dobrev D, Escande D, Nattel S, Demolombe S. Human atrial ion channel and transporter subunit gene-expression remodeling associated with valvular heart disease and atrial fibrillation. *Circulation*. 2005;112:471–481.

CLINICAL PERSPECTIVE

Excessive iron accumulation, or iron overload, is the most common monogenetic inherited disorder. It is usually caused by mutations of genes associated with ion metabolism (primary hemochromatosis) or by excessive blood transfusion required for the treatment of hereditary anemias (thalassemias and sickle cell disease). Cardiomyopathy induced by iron overload is the most common cause of mortality. This cardiomypathy is associated with bradycardia, heart block, and increased susceptibility to atrial fibrillation. The molecular and cellular mechanisms for these electrical disturbances are not known. We studied a mouse model of chronic iron overload that recapitulates the cardiomyopathy and electrical disturbances seen in humans. Iron-loaded mice have impaired intrinsic firing rates of the sinoatrial node myocytes and are most likely due to reduction in the $Ca_V1.3$-mediated L-type Ca^{2+} current ($I_{Ca,L}$). We found shifts in the current-voltage relationships of $I_{Ca,L}$ in sinoatrial node myocytes (and atrial myocytes) consistent with selective reductions in $Ca_V1.3$-mediated $I_{Ca,L}$, which is highly expressed in the sinoatrial node, atria, AV node, and proximal ventricular conduction system along with $Ca_V1.2$. By contrast, working ventricles express only $Ca_v1.2$-mediated $I_{Ca,L}$. Furthermore, mRNA for $Ca_V1.3$, but not for $Ca_V1.2$, was reduced in the atria. In addition, mice lacking $Ca_V1.3$-mediated $I_{Ca,L}$ did not show reductions in heart rate or PR-interval prolongation when treated with iron. These findings may lead to future strategies for preventing atrial remodeling and arrhythmias in patients with iron overload.

SUPPLEMENTAL MATERIAL

Iron-overload decreases Cav1.3-dependent L-type Ca^{2+} currents leading to bradycardia, altered electrical conduction and atrial fibrillation

Methods

Animals and iron-loading protocol

Five-week old male CD1 mice (Charles River Laboratories) were given an intraperitoneal (IP) injection of iron-dextran (100 mg/ml solution; 0.6 mg/g body weight dose) 3 days/week for 4 weeks. The total iron dose was 215 mg/30 g of body weight. Control mice were injected with equivalent volumes of a 10% dextrose solution. Mice with Cav1.3 ablation[26] were generated in a mixed CD1/C57B6 (50/50) background in our animal care facility by breeding heterozygous males to heterozygous females and injected with iron as described above.

All experimental procedures were performed 7 days after the last injection. Mice were housed in temperature- and humidity-controlled rooms with 12-hour light-dark cycles in the animal care facility at the University of Toronto, Department of Comparative Medicine. All experimental protocols conformed to the guidelines of the Canadian Council on Animal Care.

Telemetry electrocardiography

Five-week old male CD1 mice were anaesthetized (1% isofluorane inhalation) and implanted with radio frequency electrocardiogram (ECG) transmitters (Mouse PhysioTel® EA-F20, Data Sciences International). Transmitters were aseptically inserted into a dorsal subcutaneous tissue pocket with the positive lead of the transmitter tunnelled subcutaneously to the left anterior chest wall above the apex of the heart and the negative lead to the right shoulder.

This configuration approximates lead II on the body surface ECG. ECG recordings commenced 7 days following implantation to allow for adequate recovery from surgery.

Mice were randomly assigned to either the chronic iron overload (CIO) or control group and ECGs were recorded and monitored over a 5 week period consisting of 1 week of baseline and 4 weeks of iron loading. ECGs were acquired in 300 second intervals every 4 hours over 5 weekends (Friday 10:00 AM until Sunday at 10:00 AM) using Dataquest A.R.T. Gold acquisition software (Version 4.1, DSI). All telemetry ECG data was analyzed offline using Dataquest A.R.T. Gold analysis software (Version 4.1, DSI).

Anaesthetized mouse electrocardiography and stimulation protocols

Mice were anaesthetized (1-1.5% isofluorane inhalation) and placed on a heating pad to maintain a body temperature of 36 – 37°C. For body surface ECGs three 30 gauge subdermal needles were inserted to continuously record lead II ECGs. For intracardiac ECGs a 2 French octapolar electrode electrophysiology catheter (CIBer mouse EP catheter; NuMed Inc., Hopkinton, NY, USA) was inserted into the right jugular vein and advanced into the right atrium, through the tricuspid valve and into the right ventricle. Correct catheter placement was confirmed by having a sole ventricular signal in the distal lead, a His bundle signal in the middle lead, and a predominant atrial signal in the proximal lead. All body surface and intracardiac ECG signals were recorded and amplified at 5kHz and filtered between 0.3 Hz and 300 Hz using a Gould ACQ-7700 amplifier and the Ponemah Physiology Platform software (version 4.60, Data Sciences International).

Surface ECG allowed for the recording of standard ECG intervals (PR, RR, QRS, QT). PR interval was measured from the start of the P wave to the start of the QRS complex. QT

interval was corrected using the formula $QTc=QT/(RR/100)^{1/2}$. The His bundle electrogram was used to calculate AH and HV intervals. AH interval was measured from the start H signal to the start of the QRS complex. Several stimulation protocols were utilized in the intracardiac ECG measurements. All stimulation pulses were given at 0.4mA for 2ms, as this values was found to continuously capture and drive cardiac conduction. The baseline cycle length for stimulation was chosen to be 100ms or 20ms shorter than the mouse basal cycle length, whichever was shorter. Sinus node recovery time (SNRT) was determined following a 12 stimulus drive train, and corrected by subtracting the prestimulus RR interval (cSNRT). An 8 stimulus drive train (S1) at the set cycle length was given followed by a prestimulus (S2) for progressively shorter intervals to determine both AV node effective refractory period (AVNERP) and ventricular effective refractory period (VERP), which correspond to the shortest S1-S2 interval allowing for capture. AV Wenckebach (AV_w) and $AV_{2:1}$ conduction were determined using 8 or 18 stimulus drive trains of progressively shorter intervals until the maximum cycle length for each was reached. The ability to initiate ventricular tachycardia (VT) and ventricular arrhythmia was performed using programmed stimulation and burst pacing, whereby an 8 train burst of stimuli was followed by 3 progressively shorter prestimulus beats. VT was considered to have occurred if over 20 tachycardic ventricular beats were seen on the lead II surface electrogram. Susceptibility to VT was also studied using a 12 stimulus drive train of progressively shorter cycle lengths until the VERP was reached.

Isolation of SAN and right atrial myocytes

Mice were administered a 0.2 ml intraperitoneal injection of heparin (1000 IU/ml to prevent blood clotting and given 5 minutes for it to be absorbed. Following heparinization, mice

were anaesthetized using isofluorane (inhalation) and killed by cervical dislocation. The heart was excised into Tyrode's solution (35°C) consisting of (in mmol/L) 140 NaCl, 5.4 KCl, 1.2 KH_2PO_4, 1 $MgCl_2$, 1.8 $CaCl_2$, 5.55 glucose, 5 HEPES, and 10 IU/ml Heparin, with pH adjusted to 7.4 with NaOH. The sinoatrial node (SAN) region of the heart was isolated by separating the atria from the ventricles, cutting open the superior and inferior vanae cavae, and pinning the tissue so that the crista terminalis could be identified. The SAN area is located in the intercaval region adjacent to the crista terminalis. This SAN region was cut into strips, which were transferred and washed three times in a 'low Ca^{2+}, Mg^{2+} free' solution containing (in mmol/L) 140 NaCl, 5.4 KCl, 1.2 KH_2PO_4, 0.066 $CaCl_2$, 50 taurine, 18.5 D-glucose, 5 HEPES and 1 mg/ml bovine serum albumin (BSA), with pH adjusted to 6.9 with NaOH. SAN tissue strips were enzymatically digested for 30 minutes (35°C) in 5 ml of 'low Ca^{2+}, Mg^{2+} free' solution containing type II collagenase (254 U/ml, Worthington Biochemical Corporation, Lakewood, NJ, USA), elastase (2.3 U/ml, Worthington Biochemical Corporation) and protease type XIV (0.40 U/ml, Sigma Chemical Company), with manual agitation every 5 minutes. The tissue was then transferred and washed three times in 2.5 ml of modified KB solution (35°C) containing (in mmol/L) 100 potassium glutamate, 10 potassium aspartate, 25 KCl, 10 KH_2PO_4, 2 $MgSO_4$, 20 taurine, 5 creatine, 0.5 EGTA, 20 glucose, 5 HEPES, and 0.1% BSA, with pH adjusted to 7.4 with KOH. The tissue was transferred to 5 ml of modified KB solution and manually triturated using a fire-polished, wide-bore Pasteur pipette (inner diameter of 3 mm) until an acceptable yield of single SAN myocytes was achieved, usually within 7 minutes. Myocytes were then readapted to normal extracellular Ca^{2+} concentrations by the addition of solution containing 10 mM NaCl and 1.8 $CaCl_2$ followed by normal Tyrode's solution containing 1 mg/ml BSA. SAN myocytes were identified by their small spindle shape and ability to beat spontaneously in the

recording chamber when superfused with normal Tyrode's solution. The identical enzymatic procedure was used on tissue dissected from the right atrial appendage to isolate working right atrial myocytes. The single myocyte capacitance was 20 – 35 pF for SAN myocytes and 50 – 80 pF for right atrial myocytes.

Solutions and electrophysiological protocols

Spontaneous action potentials (APs) were recorded using the perforated patch-clamp technique[1] on single SAN myocytes. The hyperpolarization-activated current (I_f) and L-type Ca^{2+} currents ($I_{Ca,L}$) were all recorded by voltage clamping single SAN myocytes using the patch-clamp technique in the whole cell configuration.[2] APs and membrane currents were recorded at room temperature (22-23 ºC), which must be noted when comparing these data to the *in vivo* heart rate measurements.

For recording APs, and I_f the recording chamber was superfused with a normal Tyrode's solution (22 – 23ºC) containing (in mmol/L) 140 NaCl, 5 KCl, 1 $MgCl_2$, 1 $CaCl_2$, 10 HEPES, and 5 glucose, with pH adjusted to 7.4 with NaOH. The pipette filling solution for I_f contained (in mmol/L) 135 KCl, 0.1 $CaCl_2$, 1 $MgCl_2$, 5 NaCl, 10 EGTA, 4 Mg-ATP, 6.6 Na-phosphocreatine, 0.3 Na-GTP and 10 HEPES, with pH adjusted to 7.2 with KOH. Amphotericin B (200 µg/ml) was added to this pipette solution to record APs with the perforated patch clamp technique. $BaCl_2$ (1×10^{-4} mol/L) was added to the superfusate when recording I_f, in order to eliminate any inward rectifier K^+ current that could be present at low levels in some SAN myocytes.[3]

For recording $I_{Ca,L}$ SAN myocytes were superfused with a modified Tyrode's solution (22 – 23ºC) containing the following (in mmol/L) 140 CsCl, 5.4 TEA-Cl, 2 $CaCl_2$, 1 $MgCl_2$, 10

HEPES, and 5 glucose with pH adjusted to 7.4 with NaOH. The pipette solution for $I_{Ca,L}$ contained (in mmol/L) 135 CsCl, 0.1 $CaCl_2$, 1 $MgCl_2$, 5 NaCl, 10 EGTA, 4 Mg-ATP, 6.6 Na-phosphocreatine, 0.3 Na-GTP and 10 HEPES, with pH adjusted to 7.2 with CsOH. For presentation purposes some Ca^{2+} current recordings were filtered with a 60 Hz notch filter.

Micropipettes were pulled from borosilicate glass (with filament, 1.5 mm OD, 0.75 mm ID, Sutter Instrument Company) using a Flaming/Brown pipette puller (model p-87, Sutter Instrument Company). The resistance of these pipettes was 5 – 10 MΩ when filled with recording solution. Micropipettes were positioned with a micromanipulator (Burleigh PCS-5000 system) mounted on the stage of an inverted microscope (Olympus IX51). Seal resistance was 2 – 15 GΩ. Rupturing the sarcolemma in the patch for voltage clamp experiments resulted in access resistances of 5 – 15 MΩ. Series resistance compensation averaged 80 – 85% using an Axopatch 200B amplifier (Molecular Devices). For perforated patch clamp experiments access resistance was monitored for the development of capacitative transients upon sealing to the cell membrane with Amphotericin B in the pipette. Typically, access resistance became less than 40 MΩ within 5 min of sealing onto the cell, which was sufficient for recording spontaneous APs in current clamp mode. Data were digitized using a Digidata 1322A and pCLAMP 9 software (Molecular Devices) and stored on computer for *post hoc* analysis.

Activation kinetics for I_f were determined by normalizing tail currents at each voltage to the maximum current level at -160 mV and fitting the data to the Boltzmann function: $I/I_{max}=1/(1+\exp[(V_m-V_{1/2})/k])$ where V_m is the potential of the voltage clamp step, $V_{1/2}$ is the voltage at which 50% activation occurs and k is the slope factor. $I_{Ca,L}$ activation kinetics were determine by calculating chord conductance (G) with the equation $G=I/(V_m-E_{rev})$, where V_m represents the depolarizing voltages and E_{rev} is the reversal potential estimated from the current-

voltage relation of $I_{Ca,L}$. Maximum conductance (G_{max}) and $V_{1/2}$ of activation for $I_{Ca,L}$ were determined using the following function: $G=\{(V_m-V_{rev})\}\{G_{max}\}\{-1/[(1+\exp((V_m-V_{1/2})/k))+1]\}$.

mRNA and protein measurements

For mRNA measurements we used quantitative Real-Time PCR of atrial homogenates prepared by rapidly excising the heart from mice and removing the atria after which they were washed in cooled tyrode's solutions and frozen with liquid nitrogen. Frozen atria was homogenized with a Polytron in 1 mL of TRIzol Reagent to isolate mRNA using the manufacturer's instructions (Invitrogen). Residual genomic DNA was removed with DNase I (Invitrogen). RNA integrity was evaluated using a 1.2 % formaldehyde gel to assess degradation. cDNA was synthesized from 1-2 μg of RNA with random primers using the Superscript™ II Reverse Transcriptase kit (Invitrogen). The cDNA amplified by quantitative real time PCR (ViiA™ 7 Real-Time PCR System, Applied Biosystems). TaqMan probes (Applied Biosystems) were used for amplifying Cav1.2 (Mm00437917) and Cav1.3 (Mm01209927) mRNA as well as GAPDH which was used as a reference gene. All samples were loaded in triplicate. Controls reactions without cDNA template were also routinely performed and these were always negative. The differences in mRNA levels between control and iron-overloaded atria were quantified using the ΔΔCt method. Specifically, the ratio of Cav1.2 and Cav1.3 levels with the GAPDH levels (i.e. ΔCt) were estimated for the control and iron-overload samples which was then used to determine the differences between relative differences in mRNA between the samples (ΔΔCt).

Western blots were performed to estimate the level of Cav1.2 and Cav1.3 protein from atria isolated from control and iron-overloaded hearts (as above). After flash freezing in liquod nitrogen the samples were pulverized in 300μL of buffer containing 3% SDS, 50mM Tris-HCl (pH 7.5) and a protease

inhibitor cocktail (Sigma, USA). Samples were solubilised on ice for 1hr, incubated for 10min at 37°C and centrifuged for 10min (14,000rpm) at 4°C. Supernatant was then collected and total protein concentration determined using a standard Bradford assay (BioRad). 20 μg of each sample was loaded on 6% SDS-PAGE gels (25mmol/L Tris Base, 192mmol/L Glycine, 0.1% SDS), separated for 2hrs at 100mV, transferred to nitrocellulose membranes (Roche, Germany; 20mmol/L Tris Base, 150mmol/L Glycine, 20% methanol; 100V for 1hr) then blocked with 5% skim milk powder. To detect Cav1.2, nitrocellulose membranes (blots) were incubated overnight at 4°C with a rabbit polyclonal Cav1.2 (ACC005, Alomone Labs) antibody diluted 1:200. Detection was achieved using Horseradish Peroxidase-conjugated secondary rabbit antibodies (Alomone Labs) and visualized using an enhanced chemiluminescence kit (Amersham Biosciences, USA). We also attempted to measure Cav1.3 protein using the same method with a polyclonal $Ca_V1.3$ (ACC003, Alomone Labs) antbodies and antibodies kindly received from Dr. Amy Lee (U of Utah)[4] The Alomone antibodies were found to be nonspecific since they detected bands at about 270kDal in atrial lysates $Ca_V1.3$ knockout. In our conditions, the antibody from Dr. Lee[4] only gave very weak signals, which may reflect the small amounts of atrial tissue available in these studies.

Optical recordings of isolated atrial preparations

Atrial preparations were obtained from 16- to 20-wk-old female mice as follows. Mice were anesthetized. The hearts were isolated and retrogradely perfused, as described above, with a with a Tyrode's solution containing elevated KCl levels (20 mM) in order to electrically and mechanically arrest the heart. With the aid of a dissecting stereo microscope, the superior and inferior vanae cavae as well as the pulmonary veins were dissected away from the atria. Then, the atria were separated from the ventricles by carefully cutting along the annulus. The isolated atria was lightly stretched and pinned to the bottom of a Sylgard-coated 30-mm petri dish and incubated in a normal oxygenated Tyrode's solution containing the voltage-sensitive dye, 4-(2-

(6-(di-butylamino)-2-naphthalenyl)ethenyl)-1-(3-sulfopropyl)-pyridinium) hydroxide (di-4-ANEPPS; Molecular Probes, Eugene, OR), for ~10 min at a concentration of 1 μM, prepared from a 1 mg/mL stock solution in DMSO (0.1% DMSO in the final solution). The atria were then superfused at a flow rate of ~10 ml/min with Krebs solution (37°C) containing: 118.0 mM NaCl, 4.7 mM KCl, 1.2 mM KH2PO4, 1.2 mM MgSO4, 1.0 mM CaCl2, 25.0 mM NaHCO3, and 11.1 mM glucose (pH 7.4, bubbled with 95% O_2-5% CO_2). Rapid pacing with 15-20 current pulses (4 mAmps) with a duration of 2 msec were applied every 20 msecs using a platinum electrode positioned on either the right atrial appendage or right posterior atrial wall. These stimulation protocols were performed over a range of concentration of the parasympathetic agonist, carbachol (0 - 10 μM) to determine the susceptibility of the atria to atrial fibrillation which was assessed optically by illuminating di-4-ANEPPS-loaded atria with light at a wavelength of 550-570 nm (X-Cite, EXFO Life Sciences, Mississauga, ON, Canada) and recording the emitted fluorescent light (590-640 nm) using a high speed CCD camera (Cascade 128+, Photometrics, Tucson, AZ). Images were binned (64 x 64 pixels) to achieve a frame rate of 1000 frames/s. Images were captured and analyzed with ImagePro Plus 5 (Media Cybernetics, Bethesda, MD).

Results

Table SI: Echocardiographic parameters after 4 weeks of iron loading

	Control	Iron overload	P value
HR	**489 ± 13**	**364 ± 11****	**$3.4x10^{-6}$**
ESD	**2.09 ± 0.11**	**2.55 ± 0.09***	**0.026**
EDD	**3.79 ± 0.10**	**3.91 ± 0.09**	**0.582**
ESV	**14.8 ± 2.1**	**23.9 ± 2.2***	**0.026**
EDV	**62.0 ± 3.8**	**66.8 ± 3.7**	**0.632**
SV	**47.2 ± 2.5**	**42.9 ± 2.4**	**0.208**
CO	**76.4 ± 2.2**	**64.5 ± 2.0****	**0.001**
EF	**44.9 ± 2.0**	**34.9 ± 1.5***	**0.005**
FS	**23.0 ± 1.1**	**15.5 ± 0.9***	**0.005**

HR, heart rate (bpm); ESD, end-systolic diameter (mm); EDD, end-diastolic diameter (mm); ESV, end-systolic volume (µl); EDV, end-diastolic volume (µl); SV, stroke volume (µl); CO, cardiac output (ml/min); EF, ejection fraction (%); FS, fractional shortening (%). *p<0.05, **p<0.001. n = 7 for both groups. Data were analyzed by Student's t-test

Table SII: Iron accumulation, heart weight, body weight and liver weight in iron overload and control mice.

	Control	Iron overload	P value
Cardiac iron (mg/g dry weight)	**0.6 ± 0.1**	**13.1 ± 2.1***	**<0.001**
Heart weight (mg)	**192.6± 8.5**	**133.2 ± 6.0***	**<0.001**
Body weight (g)	**38.3 ± 0.55**	**26.8 ± 1.1***	**<0.001**
Heart weight/body weight (mg/g)	**5.0± 0.2**	**5.0 ± 0.1**	**0.874**
Liver weight (g)	**1.7 ± 0.1**	**2.8 ± 0.1***	**<0.001**
Liver weight/body weight (g/g)	**0.04 ± 0.001**	**0.1 ± 0.003**	**<0.001**

Data are means ± SEM; *p<0.05 vs. control; n=10-15 samples in each group. Data were analyzed by Mann-Whitney rank sum test.

Table SIII: Spontaneous action potential parameters in control and chronic iron overload sinoatrial node myocytes.

	Control	Iron overload	P value
Pacing rate (beats/min)	**138 ± 6.5**	**91.2 ± 5.4***	**$3.05x10^{-5}$**
MDP (mV)	**-68.1 ± 1.6**	**-67.7 ± 1.5**	**0.84**
Slope DD (mV/s)	**35.1 ± 3.7**	**18.8 ± 2.2***	**$3.1x10^{-5}$**
V_{max} (V/s)	**30.2 ± 3.2**	**22.0 ± 3.0**	**0.35**
OS (mV)	**27.0 ± 2.4**	**19.3 ± 2.7***	**0.04**
APD_{50} (ms)	**48.5 ± 4.9**	**28.7 ± 5.0***	**0.012**
APD_{90} (ms)	**120 ± 8.9**	**89.9 ± 8.4***	**0.025**

MDP, maximum diastolic potential; slope DD, slope of the diastolic depolarization; V_{max}, maximum action potential upstroke velocity; OS, overshoot; APD_{50}, action potential duration at 50% repolarization time; APD_{90}, action potential duration at 90% repolarization time. Data are means ± SEM; *p<0.05 vs. control; n=10 SAN myocytes in both the control and iron overload groups. Data were analyzed by Student's T-test.

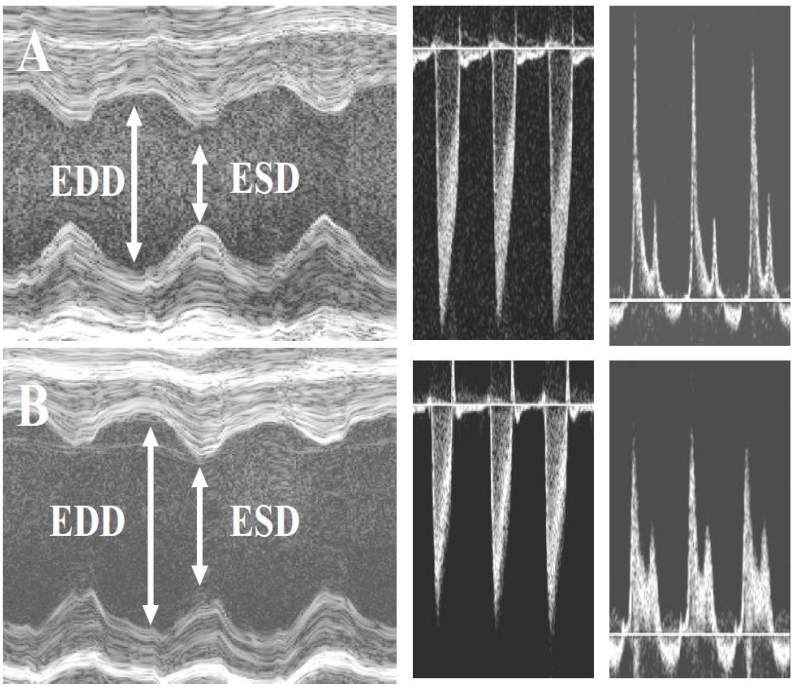

Figure S1. Functional Assessment of control and iron-overload mice. Representative M-mode echocardiograms, aortic velocity profiles and mitral valvular flows (E- and A-wave) from control (A) and iron overload (B) mice, respectively. ESD and EDD refer to the left ventricular end-systolic dimensions and end-diastolic dimensions, respectively.

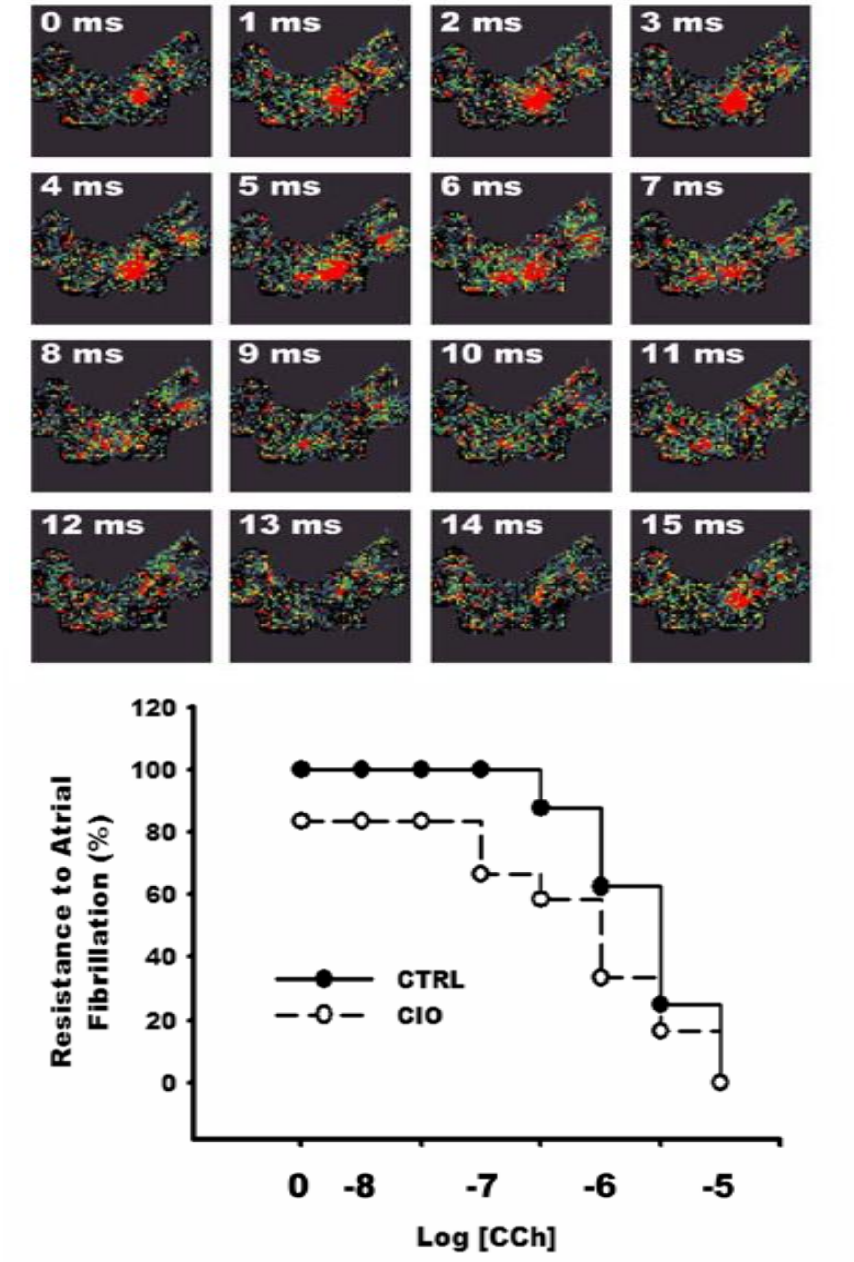

Figure S2: Atrial fibrillation in atria isolated from an iron overload mouse. The upper panel shows an example of atrial fibrillation, identified as a rapid and stable "rotor" pattern of electrical activation measured in an atrial preparation isolated from a mouse with iron-overload. In this particular case the rotor had a spontaneous frequency of electrical activity at close to 60Hz. Atrial fibrillation was induced using a rapid-pacing stimulation protocol in the presence of 100nM carbachol. The lower panel shows the percentage of isolated atria that developed sustained atrial fibrillation (i.e. rotors), lasting more than 1 minute, following program stimulation as a function of the dose of carbachol. Notice that 2 of the 10 atria isolated from CIO mice developed atrial fibrillation without carbachol treatment. Clearly, higher doses of carbachol were required in control atria versus atria isolated from CIO mice.

Reference List

1. Rae J, Cooper K, Gates P, Watsky M. Low access resistance perforated patch recordings using amphotericin B. *J Neurosci Methods* 1991;37:15-26.

2. Hamill OP, Marty A, Neher E, Sakmann B, Sigworth FJ. Improved patch-clamp techniques for high-resolution current recording from cells and cell-free membrane patches. *Pflugers Arch* 1981;391:85-100.

3. Mangoni ME, Nargeot J. Properties of the hyperpolarization-activated current (I(f)) in isolated mouse sino-atrial cells. *Cardiovasc Res* 2001;52:51-64.

4. Cui G, Meyer AC, Calin-Jageman I, Neef J, Haeseleer F, Moser T, Lee A. Ca2+-binding proteins tune Ca2+-feedback to Cav1.3 channels in mouse auditory hair cells. *J Physiol* 2007;585:791-803.